

TRIAXIAL BLACK-HOLE NUCLEI

M. Y. POON & D. MERRITT

Department of Physics and Astronomy, Rutgers University, New Brunswick, NJ 08855

Draft version October 30, 2018

ABSTRACT

We demonstrate that the nuclei of galaxies containing supermassive black holes can be triaxial in shape. Schwarzschild’s method was first used to construct self-consistent orbital superpositions representing nuclei with axis ratios of 1 : 0.79 : 0.5 and containing a central point mass representing a black hole. Two different density laws were considered, $\rho \propto r^{-\gamma}$, $\gamma = \{1, 2\}$. We constructed two solutions for each γ : one containing only regular orbits and the other containing both regular and chaotic orbits. Monte-Carlo realizations of the models were then advanced in time using an N -body code to verify their stability. All four models were found to retain their triaxial shapes for many crossing times. The possibility that galactic nuclei may be triaxial complicates the interpretation of stellar-kinematical data from the centers of galaxies and may alter the inferred interaction rates between stars and supermassive black holes.

Keywords: galaxies: elliptical and lenticular — galaxies: structure — galaxies: nuclei — stellar dynamics

1. INTRODUCTION

The phenomenon of triaxiality has remained of central importance to our understanding of galaxy dynamics since the demonstration by Schwarzschild (1979) of the existence of self-consistent triaxial equilibria. Schwarzschild’s models had large, constant-density cores and the majority of the orbits were regular, respecting three integrals of the motion. But the realization that the central densities of elliptical galaxies and bulges are very high (Crane et al. 1993), and that supermassive black holes are generic components of galaxies (Kormendy & Richstone 1995), has modified somewhat our ideas about the persistence of triaxiality. A central black hole can destroy triaxiality on large scales by rendering the center-filling box orbits stochastic (Gerhard & Binney 1985). Evolution to globally axisymmetric shapes can occur in just a few crossing times if the black hole contains of order 10^{-2} of the galaxy’s mass (Merritt & Quinlan 1998; Sellwood 2001).

Less is known about the possibility of maintaining triaxial shapes at the very centers of galaxies, where the gravitational force is contributed roughly equally by the stars and by the nuclear black hole. Regular orbits, both box-like and tube-like, exist in this region (Merritt & Valluri 1999; Sambhus & Sridhar 2000; Poon & Merritt 2001, Paper I) but the box-like orbits (the “pyramids”) have shapes that are generally contrary to the figure elongation, making them less useful than classical box orbits for maintaining a triaxial shape. Furthermore the pyramid orbits disappear within the “zone of chaos,” which begins at a radius where the enclosed stellar mass is a few times that of the black hole (Paper I), roughly 10^2 pc in a typical bright elliptical galaxy.

Here we demonstrate that triaxial equilibria do in fact exist in the vicinity of the black hole. We first (§2) use Schwarzschild’s technique to construct self-consistent superpositions of orbits computed in a fixed triaxial potential representing the stars and a central point mass. We then (§3) test the long-term stability of the models by using an N -body code to advance them forward in time; we

find that the N -body models maintain their triaxial shapes for many crossing times. Finally we present some of the observable properties of the models (§4) and discuss the implications of triaxiality for observational and theoretical studies of galactic nuclei (§5).

2. SCHWARZSCHILD SOLUTIONS

We model the stellar nucleus as a triaxial spheroid with a power-law dependence of density on radius,

$$\rho_* = \rho_0 m^{-\gamma}, \quad (1a)$$

$$m = \sqrt{\frac{x^2}{a^2} + \frac{y^2}{b^2} + \frac{z^2}{c^2}}, \quad (1b)$$

inside of some surface $m = m_{out}$ discussed below. We took $\gamma = 1$ or 2; these values correspond roughly to the density profiles observed at the centers of bright and faint elliptical galaxies, respectively (Gebhardt et al. 1996). The triaxiality T is defined as

$$T \equiv \frac{a^2 - b^2}{a^2 - c^2}. \quad (2)$$

We chose $a = 1.0, b = 0.79, c = 0.5$ for both models, corresponding to $T = 0.5$, “maximal” triaxiality. The central black hole is represented by a point mass with $M_{bh} = 1$. Expressions for the gravitational potential and forces corresponding to this mass model are given in Paper I.

Although our mass model for the stars is scale-free, the presence of the black hole imposes a scale. We identify three characteristic radii associated with the black hole. At a radius of r_g , the enclosed mass in stars (defined as the mass within an equidensity surface which intersects the x -axis at $x = r_g$) is equal to that of the black hole. In real galaxies, r_g is typically a factor of \sim a few greater than the “sphere of influence” r_h , where

$$r_h \equiv \frac{GM_{bh}}{\sigma_*^2} \approx 10.8 \text{ pc} \left(\frac{M_{bh}}{10^8 M_\odot} \right) \left(\frac{\sigma_*}{200 \text{ km s}^{-1}} \right)^{-2} \quad (3)$$

depends on the stellar velocity dispersion σ_* . The third fiducial radius is r_{ch} , the radius at which the character of

the box-like orbits undergoes a sudden transition to chaos in triaxial potentials. Table 1 gives values of r_g and r_{ch} for our two mass models; values of r_{ch} are approximate and are taken from Paper I. Table 1 also gives values of the dynamical times at r_g and r_{ch} , defined as the period of a circular orbit of the same energy in the equivalent spherical potential, defined to have a scale length $a_{ave} = (abc)^{1/3}$. The enclosed stellar mass within r_{ch} is about $3M_{bh}$ for $\gamma = 1$ and $6M_{bh}$ for $\gamma = 2$.

TABLE 1

	$\gamma = 1$	$\gamma = 2$
r_g	0.64	0.20
$T_D(r_g)$	0.98	0.17
r_{ch}	1.1	1.3
$T_D(r_{ch})$	1.8	1.5
m_{out}	5.6	3.8
$T_D(m_{out})$	5.1	4.6

Any numerical realization of a stellar system must have an outer boundary. Our goal was to test self-consistency out to a radius of at least r_{ch} , corresponding to $\sim 2r_g$ for $\gamma = 1$ and $\sim 6r_g$ for $\gamma = 2$. We therefore chose the outer surface of our mass model, $m = m_{out}$, to be large enough that almost all of the density at r_{ch} in a real galaxy would be contributed by orbits with apocenters below this surface. In order to estimate m_{out} , the isotropic distribution functions corresponding to a spherical galaxy with the density law of equation (1), $\gamma = \{1, 2\}$, and a central point mass were computed and transformed to $F(r_{apo}; r)$, the distribution of apocentric radii r_{apo} of orbits passing through r . For $\gamma = 1$, we found that orbits with $r_{apo} \lesssim 5r_{ch}$ contribute $\sim 70\%$ of the density at r_{ch} . For $\gamma = 2$, setting $r_{apo} \approx 3r_{ch}$ is sufficient to give $\sim 75\%$ of the density at r_{ch} . (r_{ch} in the spherical models was defined as the radius containing the same mass as in the triaxial models.) Our corresponding choices for m_{out} are given in Table 1.

We followed standard procedures for constructing the Schwarzschild solutions (Schwarzschild 1993; Merritt & Fridman 1996). The mass model within m_{out} was divided into 64 equidensity shells and each shell was divided into 48 cells per octant, for a total of 3072 cells. Shells were more closely spaced near the center (Figure 1). Orbits were computed in two initial condition spaces: stationary start space, which yields box-like orbits, and $X - Z$ start space, which yields mostly tube orbits. Orbital energies were selected from a grid of 42(52) values for $\gamma = 1(2)$, defined as the energies of equipotential surfaces that were spaced similarly in radius to the equidensity shells. The outermost energy shell intersected the x axis at $x = m_{out}$ for both models. Orbits were integrated for 100 dynamical times, as defined above, and their contributions to the masses in the cells were recorded. In order to distinguish regular from stochastic trajectories, the largest Liapunov exponent was computed for each orbit. For $\gamma = 1$, the total number of orbits integrated was 18144 of which 9751 were found to be regular. For $\gamma = 2$, the numbers were 22464 and 15048 respectively. Orbital weights that reproduced the masses in the 3072 cells were found via quadratic programming (e.g. Dejonghe 1989).

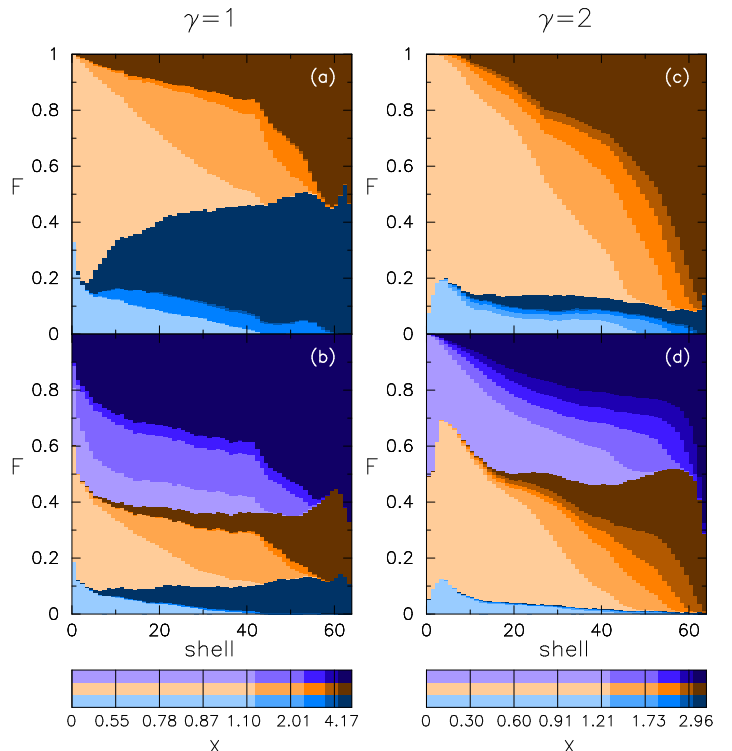


FIG. 1.— Cumulative mass fractions F contributed by different kinds of orbits to different shells of the triaxial models. Box-like orbits are green, tube orbits (both z - and x -tubes) are orange, and chaotic orbits are purple. Higher energies are indicated via darker shades; the color bar relates the shade to the radius of the equipotential surface, as explained in the text. Numbers below the color bar indicate radii where the equipotential shells intersect the x -axis. (a), (c) correspond to solutions with only regular orbits for $\gamma = 1, 2$ respectively. (b), (d) correspond to solutions with both regular and chaotic orbits.

As expected, orbital superpositions that exactly reproduced the cell masses in all of the cells, including the outermost ones, could not be found since only a few orbits visit the outer shells. We were able to find “exact” solutions (solutions which precisely reproduced the densities in a subset of cells) by relaxing the constraints in a number of ways; for instance, by eliminating the angular constraints on the outermost shells (forcing only the integrated shell mass to be fit), or by ignoring the outer cells entirely when imposing the constraints. For example, when only regular orbits were included, “exact” solutions could be found for $\gamma = 1$ for all cells within shell 51, corresponding to a radius of ~ 3.2 . This radius is substantially greater than r_{ch} (Table 1).

When these “exact” solutions were advanced forward in time, as described below, they were found to exhibit significant evolution at large radii, due to the fact that the model’s density was not correctly reproduced in the outermost cells. We therefore constructed new solutions which were not “exact,” but which were constrained to reproduce the densities in *all* cells within m_{out} with as high an accuracy as possible. Such solutions exhibited smaller fractional errors in the innermost cells ($r \lesssim r_{ch}$) than in the outer ones. Models constructed in this way were found to evolve much less than the “exact” solutions and provide the basis for the discussion below.

TABLE 2

	z -tubes	x -tubes	pyramids	chaotic
$\gamma = 1$: (regular)				
$r < 0.5$	0.61	0.10	0.29	0.00
$r < 1.0$	0.56	0.08	0.37	0.00
$r < 1.5$	0.53	0.07	0.40	0.00
$\gamma = 1$: (all)				
$r < 0.5$	0.09	0.04	0.26	0.61
$r < 1.0$	0.10	0.03	0.25	0.62
$r < 1.5$	0.10	0.02	0.25	0.63
$\gamma = 2$: (regular)				
$r < 0.4$	0.75	0.10	0.15	0.00
$r < 0.8$	0.73	0.13	0.14	0.00
$r < 1.2$	0.73	0.13	0.13	0.00
$\gamma = 2$: (all)				
$r < 0.4$	0.06	0.05	0.45	0.45
$r < 0.8$	0.05	0.05	0.44	0.47
$r < 1.2$	0.04	0.05	0.42	0.49

The orbital content of the latter solutions is described in Figure 1 and Table 2. We constructed two types of solution for each γ : solutions in which only regular orbits were used; and solutions in which all orbits (regular and chaotic) were provided to the Schwarzschild algorithm. The dominant family of orbits in the models containing only regular trajectories was found to be the z -tubes, orbits which circulate about the short axis of the figure. Plots of the individual orbits used in the solutions confirm that many of the z -tubes have the correct shape for reproducing the triaxial figure, being more elongated in x (the long axis) than in y (the intermediate axis). Most of the remaining contribution to the density of the regular nuclei was found to come from pyramid orbits and high-energy box orbits in the $\gamma = 1$ model, while for $\gamma = 2$, roughly equal contributions came from pyramid orbits and from the x -tubes. (See Paper I, Figure 1 for illustrations of the various orbit families.) The most heavily occupied pyramid orbits had shapes similar to “saucer” orbits, z -tubes associated with a $2 : 1$ resonance (Paper I, Figure 1c); both models contained roughly equal numbers of saucers and pyramids. High-energy box-like orbits are more important in the $\gamma = 1$ case than in the $\gamma = 2$ case, because: (1) high-energy tube orbits in the $\gamma = 1$ model are elongated opposite to the figure; (2) most of the high-energy regular box orbits in the $\gamma = 2$ model are bananas, which are not very useful for filling the outermost shells.

In the models constructed using both regular and chaotic trajectories, the number of stars on chaotic orbits is surprisingly high: $\sim 60\%$ for $\gamma = 1$ and $\sim 45\%$ for $\gamma = 2$ at all radii. Plots of the most highly populated chaotic orbits suggest that they have reached a nearly steady state in a time-averaged sense, filling the volume defined by the equipotential surface corresponding to their energy. Stationary chaotic building blocks like these have been used before when constructing triaxial models (e.g. Merritt & Fridman 1996) but no published triaxial models have contained nearly so large fraction of stars on chaotic orbits.

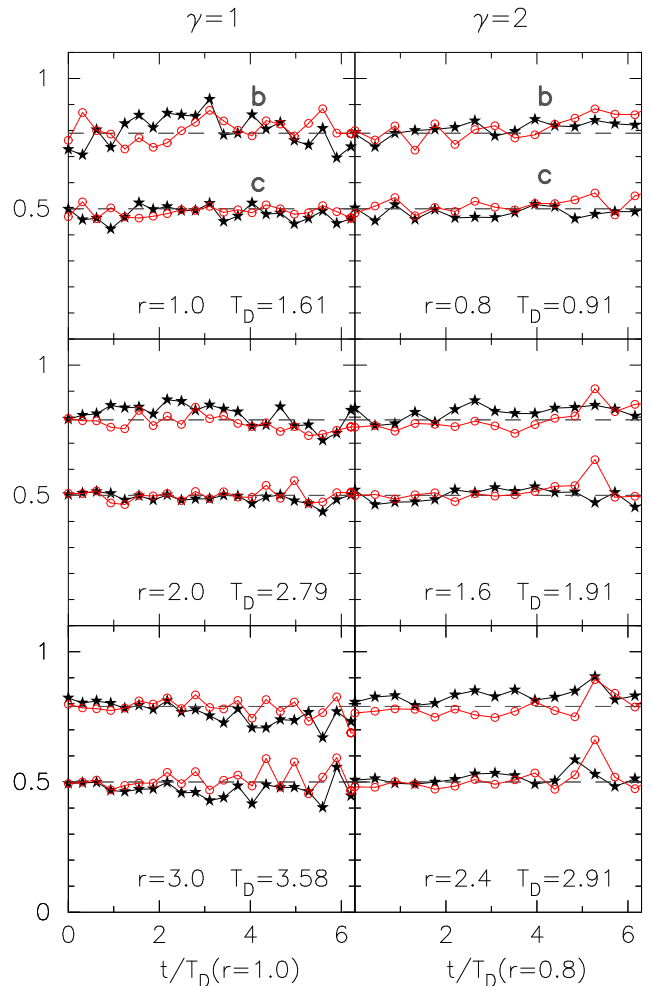


FIG. 2.— Evolution of the N -body axis ratios; $a \equiv 1$. r defines the longest dimension of the ellipsoid within which the axis ratios were determined, using the algorithm described in the text. T_D is the dynamical time at this radius. Black (red) curves correspond to solutions where only regular (both regular and chaotic) orbits were used.

3. N-BODY MODELS

We verified that our orbital superpositions correspond to true equilibria by realizing them as N -body models and integrating them forward in time in the gravitational potential computed from the N bodies themselves and from the point mass representing the black hole. Initial conditions were prepared by re-integrating all orbits with nonzero occupation numbers. The position and velocity of each trajectory were recorded at fixed time intervals; the length of each integration was determined by the orbit’s occupation number. The sense of rotation of the tube orbits was chosen randomly such that the mean motion was everywhere zero. The number of particles was 2.42×10^6 for $\gamma = 1$ and 2.19×10^5 for $\gamma = 2$; a smaller N was chosen for $\gamma = 2$ since the N -body integrations were slower for the more condensed model.

The initial conditions were then advanced in time using the N -body code GADGET (Springel, Yoshida & White 2001), a parallel tree code with variable time steps. The interparticle softening length was chosen to be 0.005 (0.003) for $\gamma = 1$ (2). Figure 2 shows the evolution of the axis ratios of the models, computed using the iterative proce-

ture described by Dubinski & Carlberg (1991). The axis ratios fluctuate with time, but the models retain their triaxial figures very well over many dynamical times. No significant evolution was seen in the radial distribution of matter.

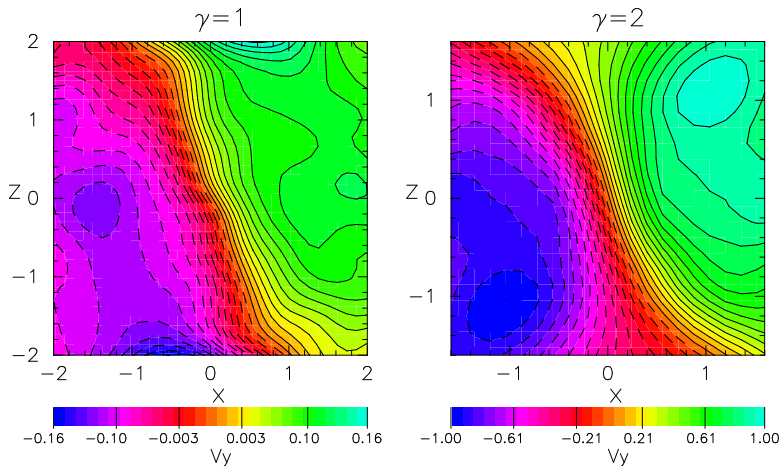


FIG. 3.— Line-of-sight velocities of the rotating regular models described in the text, as seen along the y -axis. Contours of positive (negative) velocity are represented by full (dotted) lines.

4. OBSERVABLE PROPERTIES

Two observational signatures of triaxiality are isophote twists, and kinematic misalignments. Isophote twists require a variation with radius of the intrinsic axis ratios, which is not a feature of our models. Kinematic misalignments occur whenever the intrinsic angular momentum vector does not coincide with the minor axis of the figure, and are generic features of triaxial systems when both the short- and long-axis tube orbits are populated (e.g. Franx, Illingworth & de Zeeuw 1991).

We illustrate the possibility of kinematic misalignments in our models in Figure 3. Line-of-sight velocity contours are plotted for regular models after a fraction of the x - and z -tubes were reversed, giving the models net rotation about both the long and short axes. For $\gamma = 1$, all x -tubes in Figure 3 rotate in the same sense while 60% of the z -tubes at each energy rotate in one sense and the remaining 40% in the other. For $\gamma = 2$, all x -tubes rotate in the same sense around the x axis and all z -tubes rotate in the same sense around the z -axis. Rotation of the projected models along the apparent minor axis of the figure (“minor-axis rotation”) is apparent.

5. DISCUSSION

We have shown that long-lived triaxial configurations are possible for nuclei containing black holes, whether constructed purely from regular orbits, or from a combination of regular and chaotic orbits. The latter solutions are remarkable given the large fraction of the mass on chaotic orbits, of order 50% or more (Table 2). Such solutions violate Jeans’s theorem in its standard form (e.g. Binney & Tremaine 1987) but are consistent with a generalized Jeans’s theorem (Merritt 1999) if we assume that the chaotic building blocks are “fully mixed,” that is, that they approximate a uniform population of the accessible phase space. This appears to be the case based on visual inspection of the time-averaged chaotic trajectories. While a sudden onset of chaos can effectively destroy triaxiality in models containing a large population of regular box orbits (Merritt & Quinlan 1998; Sellwood 2001), our work shows that at least the central parts of galaxies containing black holes can remain triaxial even when dominated by chaotic orbits.

Galaxy nuclei are typically modelled as oblate axisymmetric systems when deriving black hole masses from stellar-kinematical data (e.g. van der Marel et al. 1998; Joseph et al. 2001). Modelling a triaxial nucleus as axisymmetric will generally lead to biased estimates of M_{bh} ; for instance, if an elongated bar is viewed end-on, the velocity field can mimic that produced by a black hole even in the absence of a central mass concentration (Gerhard 1988). The high-resolution data on which such mass estimates are based are usually obtained from single slits, making it difficult to rule out triaxial shapes using information like that in Figure 3.

Axisymmetry is typically also assumed when deriving rates of interaction of stars with nuclear black holes (e.g. Syer & Ulmer 1999; Magorrian & Tremaine 1999). The triaxial models which we constructed from regular orbits were dominated by z -tubes (Table 2), similar to the tube orbits that populate an oblate spheroid. The rate of capture or destruction of stars by the black hole in these models would be similar to the rates in an axisymmetric nucleus. However the dominance of chaotic orbits in our second set of solutions implies a qualitatively different sort of behavior: the “loss cone” of stars captured by the black hole would be refilled on a time scale determined by the frequency of near-center passages of the chaotic orbits, rather than by two-body scattering.

This work was supported by NSF grants AST 96-17088 and 00-71099 and by NASA grants NAG5-6037 and NAG5-9046 to DM.

REFERENCES

- Binney, J. & Tremaine, S. 1987, *Galactic Dynamics* (Princeton: Princeton University Press)
- Crane, P. et al. 1993, *AJ*, 106, 1371
- Dejonghe, H. 1989, *ApJ*, 343, 113
- Dubinski, J. & Carlberg, R. 1991, *ApJ*, 378, 496
- Gebhardt, K. et al. 1996, *AJ*, 112, 105
- Gerhard, O. E. 1988, *MNRAS*, 232, 13p
- Gerhard, O. & Binney, J. J. 1985, *MNRAS*, 216, 467
- Joseph, C. L. et al. 2001, *ApJ*, 550, 668
- Kormendy, J. & Richstone, D. O. 1995, *ARAA*, 33, 581
- Magorrian, J. & Tremaine, S. 1999, *MNRAS*, 309, 447
- Franx, M., Illingworth, G. & de Zeeuw, P. T. 1991, *ApJ*, 383, 112
- Merritt, D. 1999, *PASP*, 111, 129
- Merritt, D. & Fridman, T. 1996, *ApJ*, 460, 136
- Merritt, D. & Quinlan, G. D. 1998, *ApJ*, 498, 625
- Merritt, D. & Valluri, M. 1999, *AJ*, 118, 1177
- Poon, M.Y. & Merritt, D. 2001, *ApJ*, 549, 192 (Paper I)
- Sambhus, N. & Sridhar, S. 2000, *ApJ*, 542, 143
- Schwarzschild, M. 1979, *ApJ*, 232, 236
- Schwarzschild, M. 1993, *ApJ*, 409, 563
- Sellwood, J. A. 2001, *astro-ph/0107353*
- Springel, V., Yoshida, N. & White, S. D. M. 2001, *NewA*, 6, 79
- Syer, D. & Ulmer, A. 1999, *MNRAS*, 306, 35
- van der Marel, R. P., Cretton, N., de Zeeuw, P. T., Rix, H.-W. 1998, *ApJ*, 493, 613